Bulletin of the JSME Vol.14, No.7, 2020
Journal of Advanced Mechanical Design, Systems, and Manufacturing

Method of designing gear-honing-wheel geometries
(Validation based on fundamental theory and honing experiments)

Kouji MATSUO*, Yoshitomo SUZUKI**, Junichi HONGU***,
Daisuke IBA**** and Ichiro MORIWAKI****
*Hardware System Development Department, JATCO Ltd
560-2, Okatsukoku, Atsugi City, Kanagawa 243-0126, JAPAN
E-mail: koji_matsuo@jatco.co.jp
**Engineering Management Department, JATCO Ltd
1-1, Yoshiwara, Takara-cho, Fuji City, Shizuoka 417-0023, JAPAN
***Tottori University
4-101 Koyama-cho Minami, Tottori, JAPAN
****Kyoto Institute of Technology
Goshokaido-cho, Matsugasaki, Sakyo-ku, Kyoto 606-8585, Japan

Received: 16 May 2020; Revised: 31 August 2020; Accepted: 16 September 2020

Abstract
The present paper describes a method for determining geometries of gear-honing wheels used in the final process for manufacturing automotive transmission gears. Inappropriate geometries of gear-honing wheels could cause large undulations on finished gear-tooth flanks, and the finished gear would be out of the required accuracy. In such cases, the geometries of gear-honing wheels are required to be modified iteratively until the finished gears have sufficient accuracy. The change in meshing stiffness of a gear-honing wheel and a finished gear significantly affects the rotational synchronization. The poor rotation synchronization could cause the large undulation on a finished gear-tooth flank, to be different from the target micro geometries. This paper presented a geometrical approach that was proposed for a determination method of gear-honing-wheel geometries. The method allows the meshing stiffness to be balanced. Gear-honing wheels designed with the proposed method induced the desired micro geometries of finished gear-tooth flanks in gear-honing experiments. Therefore, the proposed method with the geometrical approach could be useful for the determination of gear-honing-wheel geometries.

Keywords : Gear honing, Gear accuracy, Honing wheel, Meshing-stiffness, Number of meshing teeth

1. Introduction

Low-noise automotive transmissions are required for improving vehicle interior quietness so that gears constructing the transmissions must be manufactured at low cost and with stable quality. In response to the requirements, JATCO has gear honing as the final process following heat treatment to keep gear accuracies.

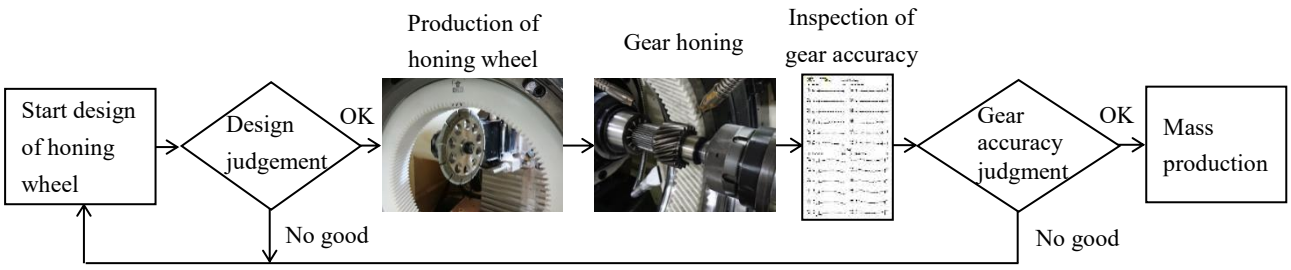

Fig. 1 Issue in gear-honing-wheel design. The geometries of honing wheels are required to be modified iteratively until the finished gears have sufficient gear accuracy.

Paper No.20-00241
[DOI: 10.1299/jamdsm.2020jamdsm0098]

Transmission gears are manufactured in a series of processes consisting of hobbing, heat treatment and honing. The accuracy of finished gears greatly depends on the geometries of the honing wheel used in the honing process. Inappropriate geometries of honing wheels could cause large undulations on finished gear-tooth flanks, and the finished gear would be out of the required accuracy. In such cases, the geometries of honing wheels are required to be modified iteratively until the finished gears have sufficient accuracy (Fig. 1).

The authors reasoned that the cause of this issue is the change in meshing stiffness of a honing wheel and a finished gear, significantly affects the rotational synchronization. The poor rotation synchronization could cause the large undulation on a finished gear-tooth flank. The change in the number of meshing teeth simultaneously is one of the most important factors that influence the meshing stiffness. The number of meshing teeth is changed during the meshing progress, it is well known in a transmission gear. Considering the meshing stiffness of the tooth pairs, the meshing stiffness is high when a large number of teeth, and the meshing stiffness becomes small when a small number of teeth (e.g., JSME Data Book, 1979; Yokoyama and Suzuki, 1998). As described above, due to the meshing stiffness changes with the constant period as the meshing progress, the amount of teeth deflection also changes resulting in transmission error will be occurred (Kubo and Umezawa, 1977).

On the other hand, considering the honing process, the meshing condition is repeated while the number of meshing teeth changes with the meshing progress between a honing wheel and a target gear. Gear honing is a method of processing the left and right tooth flanks with tight meshing. Therefore, when there is a difference in the number of meshing teeth on the left and right tooth flanks, the difference in the meshing stiffness of the left and right tooth flanks will be occurred. This could cause the difference deflection between the left and right tooth flanks, cause the poor rotational synchronization. In other words, the poor rotational synchronization could cause the surface pressure fluctuations on the left and right tooth flanks, resulting in the finished tooth flank has large undulation. Based on the above, if the poor rotational synchronization can be improved by meshing in the condition that the meshing stiffness between the left and right tooth flanks is no difference, the tooth-flank undulations can be improved. In this study, the condition that there is no difference in the meshing stiffness between the left and right tooth flanks is called the meshing-stiffness balance, and to clarify the method of designing honing-wheel geometries for optimizing the meshing-stiffness balance.

Internal gear honing has invented approximately thirty years ago, it has been investigated in previous studies, include development of gear honing machine (Ueno et al., 2001), (Schnider, 2009), studies on surface roughness (Metha and Rathi, 2013), (Rares and Dana, 2018), gear honing processing conditions (Klocke et al., 2009), (Klocke et al., 2014), (Bergs, 2018), (Pascalau et al., 2018) and design of honing wheel (e.g., Gunbara and Takenoshita, 2003). Among these studies, Klocke et al. focused on the difference between the total contact line length variation during the honing and the total contact line length between the left and right tooth flanks. And reported that the smaller the variation in the total contact line length between the left and right tooth flanks, can be more stable the machining. It is mentioned that the difference in the total contact line length between the left and right tooth flanks decreases as the diameter of the target gear increases (Klocke et al., 2009), (Klocke et al., 2014). However, effect of honing-wheel geometries are not clarified against it. On the other hand, in the studies of Gunbara et al., a method of determining the changed shaft angle at every tooth flank dressing in order to suppress changes in the micro geometries of the target gear from the new honing wheel until the honing-wheel tool life (Gunbara et al., 2000) (Gunbara, 2003) (Gunbara et al., 2003). Other studies investigated methods of determining the number of honing wheel teeth and the helix angle in order to increase the number of times the honing wheel is dressed until the honing-wheel tool life (Gunbara et al., 2001) (Gunbara and Takenoshita, 2003), but these are no design methods that are focused on optimizing the meshing-stiffness balance.

Therefore, a geometrical approach was applied in this study with the aim of proposing a method of designing honing-wheel geometries so as to optimize the meshing-stiffness balance. Specifically, a fundamental meshing equation was derived for internal gear honing, and the geometrical positional relationship between the tool and the target gear was determined. A method was developed for analyzing the tooth-flank micro geometry in internal gear honing in which machining proceeds under line-contact meshing of the tool and the target gear in this positional relationship. Then, based on this tooth-flank micro geometry analysis method, a honing-wheel-design method was proposed for optimizing the meshing-stiffness balance between the honing wheel and the target gear during the honing process. Honing experiments were then conducted to validate the design method. In addition, the issue of whether honing-wheel geometries should be designed taking into account tooth-flank modifications to be applied to the target gear was also investigated because the influence of such modifications was unclear. As a result, a honing-wheel-design method was proposed that suppresses tooth-flank undulations, and its validity was verified in honing experiments.

[DOI: 10.1299/jamdsm.2020jamdsm0098]

2. Fundamental analysis of meshing in internal gear honing

As shown in Fig. 2, internal gear honing is done with an internal honing wheel by meshing the target gear and the honing wheel under the application of a center distance a and a shaft angle Σ to generate relative sliding of their tooth flanks along the tooth profile and along the tooth helix. Gear honing is performed after heat treatment to finish the target-gear-tooth flank to its desired micro geometry. The target-gear-tooth flank is machined under line-contact meshing of the honing wheel and the target gear.

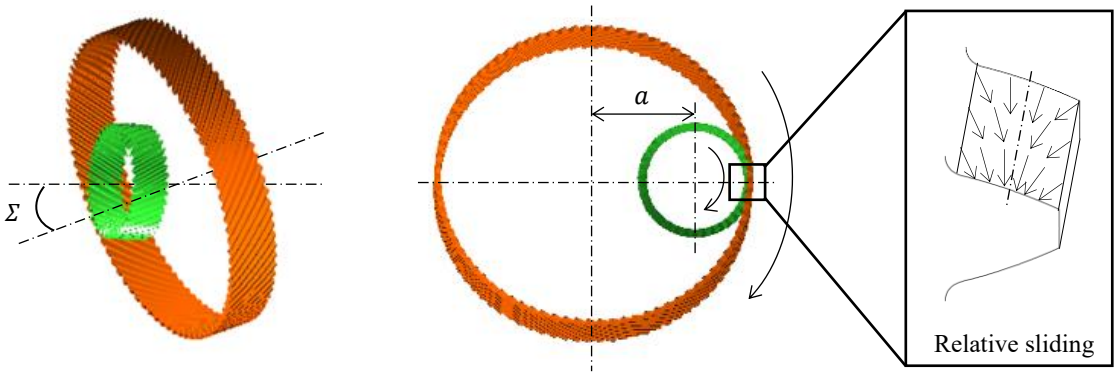

Fig. 2 Positional relationship between internal gear honing tool and target gear. The yellow-green shows target gear and the brown indicates honing wheel that has internal teeth. A shaft angle Σ and a center distance is indicated as notation a. When the rotational direction of target gear and honing wheel is clockwise, the relative sliding velocity vector of target gear during the honing is denoted by arrows in the figure.

Because the target gear and honing wheel are meshed in this way in internal gear honing by applying a shaft angle, it can be regarded as one type of crossed helical gear meshing. However, the calculation equation for crossed helical gears is based on point-contact meshing. In addition, complex 3D interference occurs on the target-gear-tooth flank in meshing with the internal gear. Because line-contact meshing actually occurs in the honing process, the meshing state during honing cannot be calculated accurately with a simple calculation for crossed helical gear meshing.

Therefore, this section explains the derivation of a fundamental meshing equation for internal gear honing based on the equation for calculating crossed helical gear meshing and describes the determination of the geometrical positional relationship between the honing wheel and the target gear. In section 3, a tooth-flank micro geometry analysis method is proposed for internal gear honing performed under line-contact meshing in order to accurately calculate meshing during the honing process.

2.1 Derivation of fundamental meshing equation for internal gear honing

Nakata (Nakata, 1949) presented a fundamental meshing equation for non-backlash meshing of two external gears having different helix angles on the base circle. However, no equation was presented for meshing with an internal gear. Therefore, in this section we will derive a fundamental meshing equation for non-backlash meshing of an internal gear and an external gear having different helix angles on the base circle.

It is assumed here that the internal and external gears share the same normal module m_n and normal pressure angle α_n. Figure 3 shows the meshing state of the internal and external gears when engaged without any backlash. Based on the meshing state in Fig. 3, the meshing calculation proceeds under the condition where the sum of s_{wn1} and s_{wn2} of both gears in the working band is equal to p_{wn}. In other words, the following equation holds true.

$$p_{wn} = s_{wn1} + s_{wn2} \tag{1}$$

p_{wt1} and p_{wt2} are calculated with the following equations.

$$p_{wt1} = \frac{d_{b1}}{\cos \alpha_{wt1}} \frac{\pi}{z_1} \tag{2}$$

$$p_{wt2} = \frac{d_{b2}}{\cos \alpha_{wt2}} \frac{\pi}{z_2} \tag{3}$$

[DOI: 10.1299/jamdsm.2020jamdsm0098]

Here, d_b is the base circle diameter and z is the number of gear teeth. From Fig. 3, p_{wt1} and p_{wt2} are converted to normal pitch values that are geometrically the same as p_{wn}. From this relationship, the following equation can be derived.

$$p_{wn} = \frac{d_{b1}}{\cos\alpha_{wt1}}\frac{\pi}{z_1}\cos\beta_{w1} = \frac{d_{b2}}{\cos\alpha_{wt2}}\frac{\pi}{z_2}\cos\beta_{w2} \tag{4}$$

From the relationship in Eq. (4), the following equation can be derived.

$$\frac{d_{b2}}{\cos\alpha_{wt2}}\cos\beta_{w2} = \frac{z_2}{z_1}\frac{d_{b1}}{\cos\alpha_{wt1}}\cos\beta_{w1} \tag{5}$$

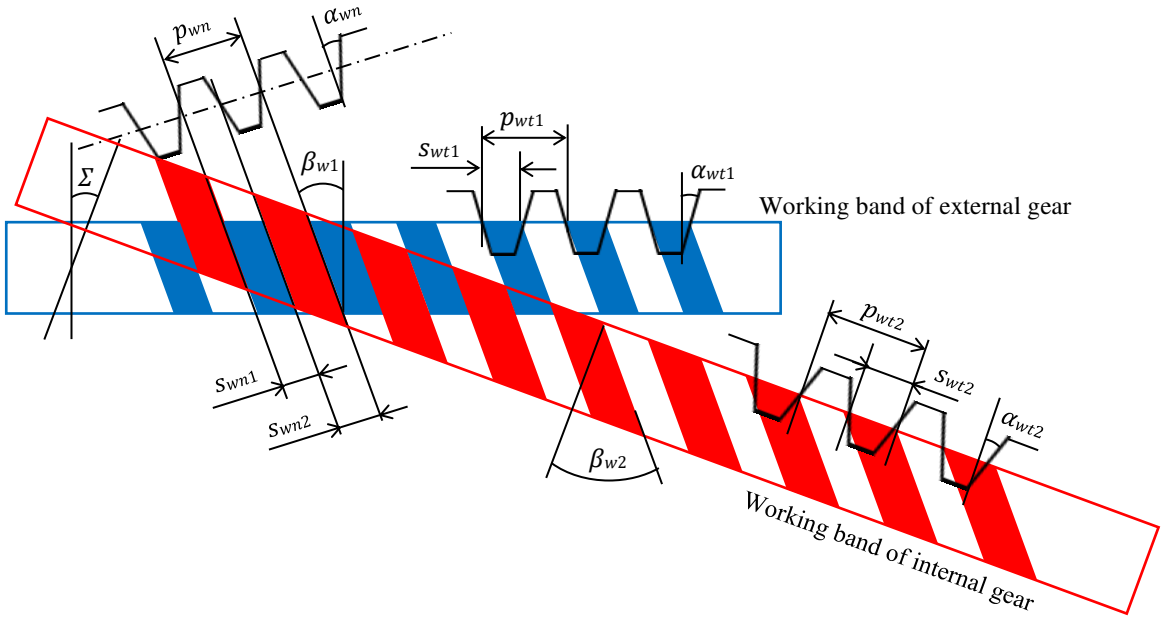

Fig. 3 Diagram of meshing condition in internal gear honing. The blue shows working band of external gear that is target gear, and the red shows working band of internal gear that is honing wheel. The notation α_{wt} is the working transverse pressure angle, s_{wt} is the transverse tooth thickness in the working band, p_{wt} is the transverse pitch in the working band, α_{wn} is the working normal pressure angle, p_{wn} is the normal pitch in the working band, s_{wn} is the normal tooth thickness in the working band, β_w is the helix angle in the working band (right-handed helix is positive, left-handed helix is negative), Σ is the shaft angle, subscript 1 denotes the external gear and subscript 2 denotes the internal gear.

Next, s_{wn1} and s_{wn2} are calculated with the following equations using the profile shift coefficient x_n and the transverse pressure angle α_t.

$$s_{wn1} = \left(\frac{\frac{\pi}{2}+2x_{n1}\tan\alpha_n}{z_1} + inv\alpha_{t1} - inv\alpha_{wt1}\right)\frac{d_{b1}}{\cos\alpha_{wt1}}\cos\beta_{w1} \tag{6}$$

$$s_{wn2} = \left(\frac{\frac{\pi}{2}+2x_{n2}\tan\alpha_n}{z_2} - inv\alpha_{t2} + inv\alpha_{\omega t2}\right)\frac{d_{b2}}{\cos\alpha_{wt2}}\cos\beta_{w2} \tag{7}$$

Substituting Eq. (6) and Eq. (7) into Eq. (1) and reorganizing the expression using the relationship in Eq. (5) makes it possible to derive the following equation.

$$-z_1(inv\alpha_{wt1} - inv\alpha_{t1}) + z_2(inv\alpha_{wt2} - inv\alpha_{t2}) = -2\tan\alpha_n\,(x_{n1} + x_{n2}) \tag{8}$$

However, because Eq. (8) has two unknown quantities, α_{wt1} and α_{wt2}, on the left-hand side, the following geometrical relationship between the transverse pressure angle and the normal pressure angle

[DOI: 10.1299/jamdsm.2020jamdsm0098]

$$\sin\alpha_{wt1} = \frac{\sin\alpha_{wn}}{\cos\beta_{b1}} \tag{9}$$

$$\sin\alpha_{wt2} = \frac{\sin\alpha_{wn}}{\cos\beta_{b2}} \tag{10}$$

is used to create one unknown quantity, α_{wn}. Substituting Eqs. (9) and (10) into Eq. (8) makes it possible to derive the following equation.

$$-z_1\left\{inv\left(\sin^{-1}\left(\frac{\sin\alpha_{wn}}{\cos\beta_{b1}}\right)\right) - inv\alpha_{t1}\right\} + z_2\left\{inv\left(\sin^{-1}\left(\frac{\sin\alpha_{wn}}{\cos\beta_{b2}}\right)\right) - inv\alpha_{t2}\right\} = -2\tan\alpha_n(x_{n1}+x_{n2}) \tag{11}$$

This Eq. (11) is referred to as the fundamental meshing equation of internal gear honing. An arbitrary initial value is applied to the unknown quantity α_{wn} on the left-hand side of the equation and a convergence calculation is performed to calculate α_{wn} that agrees with the value on the right-hand side.

2.2 Center distance

The shortest center distance a is calculated with the following equation.

$$a = \frac{d_{b2}}{2\cos\alpha_{wt2}} - \frac{d_{b1}}{2\cos\alpha_{wt1}} \tag{12}$$

2.3 Shaft angle

The shaft angle Σ is calculated with the following equation based on the helix angle in the working band β_w.

$$\Sigma = \beta_{w1} - \beta_{w2} \tag{13}$$

Here, using the geometrical relationship between the helix angle on the base circle β_b and the working transverse pressure angle α_{wt},

$$\tan\beta_{b1} = \cos\alpha_{wt1}\tan\beta_{w1} \tag{14}$$

$$\tan\beta_{b2} = \cos\alpha_{wt2}\tan\beta_{w2} \tag{15}$$

the following equation can be derived.

$$\Sigma = \tan^{-1}\left(\frac{\tan\beta_{b1}}{\cos\alpha_{wt1}}\right) - \tan^{-1}\left(\frac{\tan\beta_{b2}}{\cos\alpha_{wt2}}\right) \tag{16}$$

3. Analysis tooth-flank micro geometry in internal gear honing

Next, we will propose a method of analysis the tooth flank in internal gear honing in which machining proceeds under line-contact meshing. The aim of this method is to correctly analysis meshing during honing. Tooth-flank modification is applied to automotive transmission gears to meet the requirements for strength and noise, vibration and harshness (NVH) performance. Methods of analyzing the tooth flank during honing have been studied previously (Gunbara, 2004), (Moriwaki et al., 2004), (Gunbara, 2005), but tooth-flank modifications were not taken into account. Therefore, the analysis method proposed here has been developed to take into account tooth-flank deviations, i.e., gear accuracy represented by tooth profile slope deviation ($f_{H\alpha}$), tooth profile form deviation ($f_{f\alpha}$), tooth helix slope deviation ($f_{H\beta}$), and amount of flank line crowning (C_β). It addition, it can also treat tooth flank twist.

3.1 Expression of tooth-flank deviation

The proposed analysis method expresses tooth-flank deviation in terms of an nth-order polynomial interpolation in order to be able to treat complex tooth-flank modification. The following procedure is used to express tooth-flank

[DOI: 10.1299/jamdsm.2020jamdsm0098]

deviation.

(1) As shown in Fig. 4, tooth-flank deviation is calculated on grid points based on $f_{H\alpha}$, $f_{f\alpha}$, $f_{H\beta}$, C_β and amount of flank twist of the target gear.

(2) A polynomial coefficient along the tooth profile is calculated by solving an $(n+1)$ original simultaneous linear equation from the leading and trailing grid points $(n+1)$ along the tooth profile, including a certain grid point ij, where x is the theoretical normal length, y is the tooth-flank deviation and k_{1ij} to $k_{(n+1)ij}$ is the polynomial coefficient. This is referred to as the tooth-profile interpolation function SP. Similarly, a polynomial coefficient along the tooth helix is calculated by solving an $(n+1)$ original simultaneous linear equation where x is the face width position, y is the tooth-flank deviation and h_{1ij} to $h_{(n+1)ij}$ is the polynomial coefficient. This is referred to as the tooth-helix interpolation function SL.

(3) The nth-order polynomial coefficients along the tooth profile and tooth helix are calculated at all grid points ij. The order and number of grid divisions of a polynomial interpolation are arbitrary, but it is noted that in this study the order of the polynomial interpolation was set at n = 5 and the number of divisions along both the tooth profile and tooth helix was set at 50.

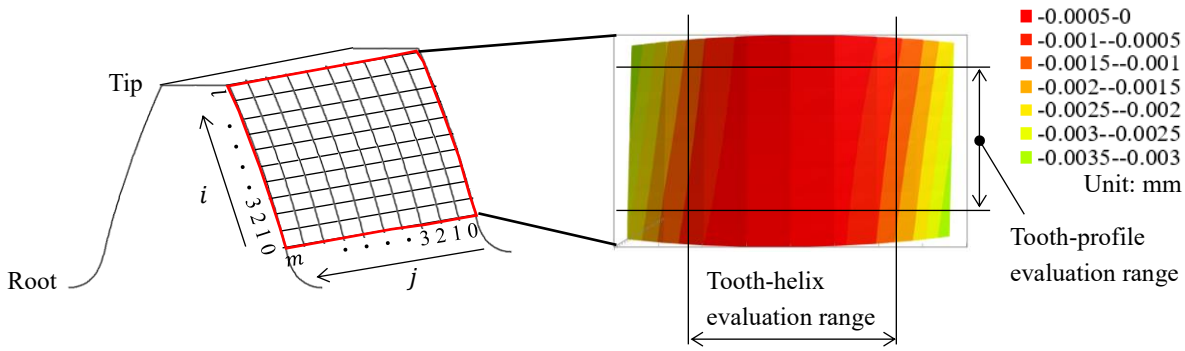

Fig. 4 Tooth-flank deviation as seen on grid points. Tooth-profile direction grid point number is indicated as i, and tooth-helix direction grid point number is indicated as j. At the each grid point ij have deviation by amount of $f_{H\alpha}$, $f_{f\alpha}$, $f_{H\beta}$, C_β and amount of flank twist of the target gear. $f_{H\alpha}$ and $f_{f\alpha}$ are given by tooth-profile evaluation range, $f_{H\beta}$ and C_β are given by tooth-helix evaluation range. The amount of flank twist is given by difference of $f_{H\alpha}$ at both ends of the tooth-helix evaluation range.

The tooth-profile interpolation function along the tooth profile at grid point ij, SP_{ij}, can be expressed as shown below using k_{1ij} to $k_{(n+1)ij}$ as the nth-order polynomial coefficient.

$$SP_{ij} = k_{1ij} + k_{2ij}\ (r_b \tan\alpha_{at}) + k_{3ij}(r_b \tan\alpha_{at})^2 + \cdots + k_{(n+1)ij}(r_b \tan\alpha_{at})^n \tag{17}$$

where r_b is the base circle radius and α_{at} is the transverse pressure angle at an arbitrary radius.

Next, the tooth-helix interpolation function along the tooth helix at grid point ij, SL_{ij}, can be expressed as shown below using h_{1ij} to $h_{(n+1)ij}$ as the nth-order polynomial coefficient.

$$SL_{ij} = h_{1ij}{}' + h_{2ij}w + h_{3ij}w^2 + \cdots + h_{(n+1)ij}w^n \tag{18}$$

$$h_{1ij}{}' = h_{1ij} - (h_{1ij} + h_{2ij}w + h_{3ij}w^2 + \cdots + h_{(n+1)ij}w^n) \tag{19}$$

Where w is an arbitrary face width position. Substituting Eq. (19) into Eq. (18) yields an apparent zero, but this equation cannot be eliminated because it is needed for calculating the tooth flank normal vector in subsection 3.3. The tooth-flank deviation ε_{ij} at grid point ij is expressed as

$$\varepsilon_{ij} = SP_{ij} + SL_{ij} \tag{20}$$

It is noted that if SP_{ij} or SL_{ij} is used, the tooth-flank deviation can also be calculated for an arbitrary radius or face width position, not just at a given grid point.

[DOI: 10.1299/jamdsm.2020jamdsm0098]

3.2 Establishment of coordinate systems

Figure 5 shows the right-hand coordinate systems of the target gear and the honing wheel. The coordinate system of the target gear is represented by X_1, Y_1, Z_1 and that of the honing wheel by X_2, Y_2, Z_2.

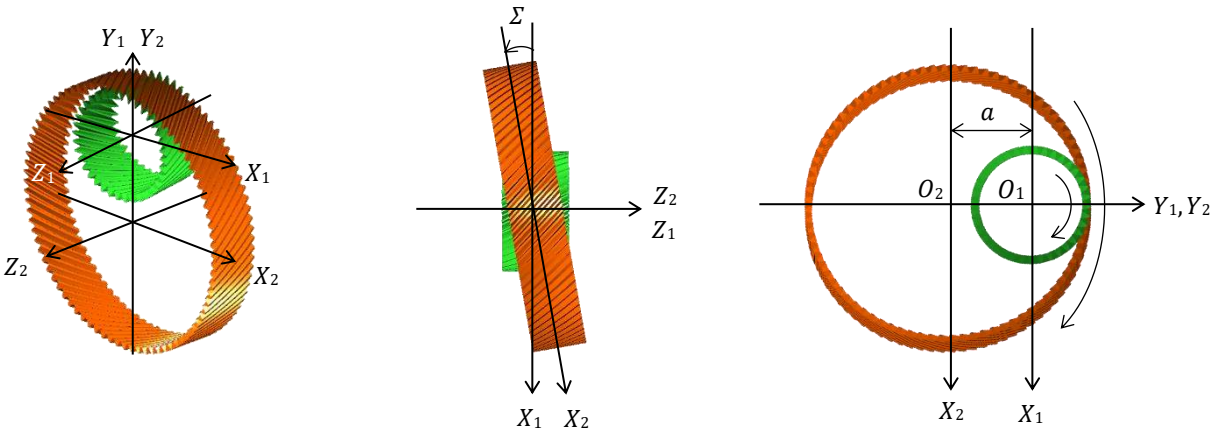

Fig. 5 Coordinate systems of target gear and honing wheel. The notation a is the center distance, Σ is the shaft angle, and the directions indicated by the arrows are assumed to be positive (+). The target gear is assumed to rotate clockwise.

3.2.1 Conversion of target-gear coordinate system to honing-wheel coordinate system

Based on Fig. 2, the following equation is valid for converting the coordinate system of the target gear to that of the honing wheel.

$$\begin{bmatrix} x_2 \\ y_2 \\ z_2 \\ 1 \end{bmatrix} = \begin{bmatrix} \cos\Sigma & 0 & \sin\Sigma & 0 \\ 0 & 1 & 0 & a \\ -\sin\Sigma & 0 & \cos\Sigma & 0 \\ 0 & 0 & 0 & 1 \end{bmatrix} \begin{bmatrix} x_1 \\ y_1 \\ z_1 \\ 1 \end{bmatrix} \tag{21}$$

3.2.2 Conversion of honing-wheel coordinate system to target-gear coordinate system

Similarly, the following equation is valid for converting the coordinate system of the honing wheel to that of the target gear.

$$\begin{bmatrix} x_1 \\ y_1 \\ z_1 \\ 1 \end{bmatrix} = \begin{bmatrix} \cos\Sigma & 0 & -\sin\Sigma & 0 \\ 0 & 1 & 0 & -a \\ \sin\Sigma & 0 & \cos\Sigma & 0 \\ 0 & 0 & 0 & 1 \end{bmatrix} \begin{bmatrix} x_2 \\ y_2 \\ z_2 \\ 1 \end{bmatrix} \tag{22}$$

3.3 Method of analyzing the honing-wheel-tooth flank from the target-gear-tooth flank

Figure 6 shows the definitions of various parameters that are used in analyzing the honing-wheel-tooth flank micro geometry from the target-gear-tooth flank micro geometry. The notation ψ_{b1} in Fig. 6 is calculated with the following equation.

$$\psi_{b1} = \frac{s_{bt1}}{d_{b1}} \tag{23}$$

[DOI: 10.1299/jamdsm.2020jamdsm0098]

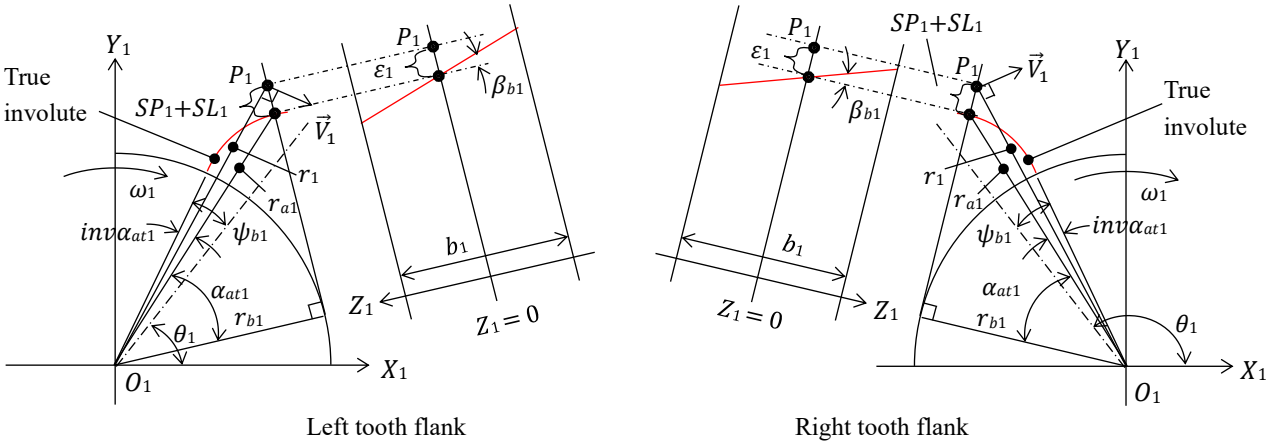

Fig. 6 Definitions of various parameters. The notation r_{b1} is the base circle radius, β_{b1} is the helix angle on the base circle (right-handed helix is positive, left-handed helix is negative), at grid point ij, r_{a1} is the radius, α_{at1} is the transverse pressure angle on r_{a1}, SP_1+SL_1 indicates the tooth-flank deviation, $P_1(P_{x1}, P_{y1}, P_{z1})$ is an tooth-flank coordinate, r_1 is the radius of P_1, $\overrightarrow{V_1}(V_{x1}, V_{y1}, V_{z1})$ is the velocity vector of P_1, ψ_{b1} is the half angle of the transverse arc tooth thickness on the base circle, θ_1 is the tooth thickness center angle from the X_1 axis on the $Z_1 = 0$ cross section, and ω_1 is the angular velocity (for clockwise rotation).

Where s_{bt1} is the transverse arc tooth thickness on the base circle and d_{b1} is the diameter of the base circle.

The coordinates are calculated with the following equations, taking into account that the involute origin is offset by $w_1 tan\beta_{b1}/r_{b1}$ relative to the $Z_1 = 0$ cross section and also the tooth-flank deviation. Here w_1 is the face width position.

In the case of the right tooth flank:

$$P_{x1} = r_{a1}\cos\left(\theta_1 - \psi_{b1} + inv\alpha_{at1} + w_1\frac{\tan\beta_{b1}}{r_{b1}}\right) + (SP_1 + SL_1)\sin(\theta_1 - \psi_{b1} + \tan\alpha_{at1} + w_1\frac{\tan\beta_{b1}}{r_{b1}}) \quad (24)$$

$$P_{y1} = r_{a1}\sin\left(\theta_1 - \psi_{b1} + inv\alpha_{at1} + w_1\frac{\tan\beta_{b1}}{r_{b1}}\right) - (SP_1 + SL_1)\cos(\theta_1 - \psi_{b1} + \tan\alpha_{at1} + w_1\frac{\tan\beta_{b1}}{r_{b1}}) \quad (25)$$

$$P_{z1} = \ w_1 \quad (26)$$

In the case of the left tooth flank:

$$P_{x1} = r_{a1}\cos\left(\theta_1 + \psi_{b1} - inv\alpha_{at1} + w_1\frac{\tan\beta_{b1}}{r_{b1}}\right) - (SP_1 + SL_1)\sin(\theta_1 + \psi_{b1} - \tan\alpha_{at1} + w_1\frac{\tan\beta_{b1}}{r_{b1}}) \quad (27)$$

$$P_{y1} = r_{a1}\sin\left(\theta_1 + \psi_{b1} - inv\alpha_{at1} + w_1\frac{\tan\beta_{b1}}{r_{b1}}\right) + (SP_1 + SL_1)\cos(\theta_1 + \psi_{b1} - \tan\alpha_{at1} + w_1\frac{\tan\beta_{b1}}{r_{b1}}) \quad (28)$$

$$P_{z1} = \ w_1 \quad (29)$$

The radius r_1 of P_1 and $\overrightarrow{V_1}$ are calculated with the following equations.

$$r_1 = \sqrt{{P_{x1}}^2 + {P_{y1}}^2} \quad (30)$$

$$\vec{V}_1 = (V_{x1},\ V_{y1},\ V_{z1}) = \left\{\ r_1\omega_1\cos\left(\tan^{-1}\frac{P_{y1}}{P_{x1}} - \frac{\pi}{2}\right),\ r_1\omega_1\sin\left(\tan^{-1}\frac{P_{y1}}{P_{x1}} - \frac{\pi}{2}\right),\ 0\ \right\} \quad (31)$$

The normal vector $\overrightarrow{V_1}$ of P_1 is calculated with the following equation from the outer product and by partial differentiation of P_1 by the parameters α_{at1} and w_1.

$$\vec{N}_1 = (N_{x1},\ N_{y1},\ N_{z1}) = \frac{\partial P_1}{\partial \alpha_{at1}} \times \frac{\partial P_1}{\partial w_1} = \left(\frac{\partial P_{y1}}{\partial \alpha_{at1}}\frac{\partial P_{z1}}{\partial w_1} - \frac{\partial P_{y1}}{\partial w_1}\frac{\partial P_{z1}}{\partial \alpha_{at1}}, \frac{\partial P_{x1}}{\partial w_1}\frac{\partial P_{z1}}{\partial \alpha_{at1}} - \frac{\partial P_{x1}}{\partial \alpha_{at1}}\frac{\partial P_{z1}}{\partial w_1},\right.$$
$$\left.\frac{\partial P_{x1}}{\partial \alpha_{at1}}\frac{\partial P_{y1}}{\partial w_1} - \frac{\partial P_{x1}}{\partial w_1}\frac{\partial P_{y1}}{\partial \alpha_{at1}}\right) \quad (32)$$

The unit normal vector $\overrightarrow{n_1}$ of P_1 is calculated with the following equation.

[DOI: 10.1299/jamdsm.2020jamdsm0098]

$$\vec{n}_1 = (n_{x1},\ n_{y1},\ n_{z1}) = \left(\frac{N_{x1}}{\sqrt{{N_{x1}}^2+{N_{y1}}^2+{N_{z1}}^2}}, \frac{N_{y1}}{\sqrt{{N_{x1}}^2+{N_{y1}}^2+{N_{z1}}^2}}, \frac{N_{z1}}{\sqrt{{N_{x1}}^2+{N_{y1}}^2+{N_{z1}}^2}} \right) \tag{33}$$

Here, in Eq. (21), P_1 is converted to P_2 in the honing-wheel coordinate system. The radius r_2 and velocity vector $\overrightarrow{V_2}$ of P_2 are calculated with the following equations where ω_2 is the angular velocity, z_1 is the number of dressing gear teeth and z_2 is the number of honing-wheel teeth.

$$r_2 = \sqrt{{P_{x2}}^2 + {P_{y2}}^2} \tag{34}$$

$$\omega_2 = \omega_1 \frac{z_1}{z_2} \tag{35}$$

The velocity vector $\overrightarrow{V_2}$ of P_2 is calculated with the following equation.

$$\vec{V}_2 = (V_{x2},\ V_{y2},\ V_{z2}) = \left\{ r_2\omega_2 \cos\left(\tan^{-1}\frac{P_{y2}}{P_{x2}} - \frac{\pi}{2}\right),\ r_2\omega_2 \sin\left(\tan^{-1}\frac{P_{y2}}{P_{x2}} - \frac{\pi}{2}\right),\ 0 \right\} \tag{36}$$

Next, $\overrightarrow{V_2}$ is converted to the target gear coordinate system in the following equation and expressed as $\vec{V}_2{}'$.

$$\vec{V}_2{}' = (V_{x2}',\ V_{y2}',\ V_{z2}') = \left(V_{x2}\cos\Sigma,\ V_{y2},\ V_{x2}\sin\Sigma\right) \tag{37}$$

The honing-wheel-tooth-flank coordinate P_2 that corresponds to P_1 has an origin angle of θ_1 where the internal product of the unit normal vector $\overrightarrow{n_1}$ and the relative velocity vector $\vec{V}_1 - \vec{V}_2{}'$ is zero. In other words,

$$\vec{n}_1 \cdot \left(\vec{V}_1 - \vec{V}_2{}'\right) = \left\{ n_{x1}\left(\vec{V}_{x1} - \vec{V}_{x2}{}'\right) + n_{y1}\left(\vec{V}_{y1} - \vec{V}_{y2}{}'\right) + n_{z1}\left(\vec{V}_{z1} - \vec{V}_{z2}{}'\right) \right\} = 0 \tag{38}$$

θ_1 is calculated with a convergence calculation that satisfies the condition above. If the honing-wheel-tooth-flank coordinates P_2 are calculated for all the corresponding P_1 grid points using Eqs. (24) to (38), the honing-wheel-tooth flank corresponding to the target-gear-tooth flank can be analyzed. Especially, important point is that the tooth flank in internal gear honing in which machining proceeds under line-contact meshing can be analyzed by using calculated θ_1.

3.5 Analysis example

This subsection presents an example of an analysis that was performed with the foregoing analysis method, assuming a secondary reduction gear of a CVT used on midsized vehicles and no tooth-flank modification of the target gear. Table 1 shows the specifications of the target gear and the honing wheel.

Table 1 Specifications of target gear and honing wheel

			Target gear	Honing wheel
Module	m_n	mm	2.41	←
Pressure angle	α_n	deg.	18.5	←
Helix angle	β	deg.	31.0 (LH)	40.86(LH)
Number of teeth	z	-	23	97
Tip diameter	d_a	mm	73.2	308.4
Root diameter	d_f	mm	58.72	322.4
Profile shift coeff.	x_n	-	0.35	-1.27
Face width	B	mm	35.9	50
Shaft angle	Σ	deg.	10.00	

Figure 7 presents contour diagrams showing the θ_1 on the grid points of the right and left tooth flanks. This figure enables an analysis of the position of the line of contact appearing on the right and left tooth flanks during honing that

[DOI: 10.1299/jamdsm.2020jamdsm0098]

corresponds to the rotation of the target gear. In this analysis example, it is seen that honing begins from the bottom and tooth root side of the right tooth flank and then after clockwise rotation of 7.86 deg. (= 126.77 – 118.91 deg.) honing begins from the bottom and tooth tip side of the left tooth flank. This rotation angle difference is referred to as the meshing phase difference between the right and left tooth flanks.

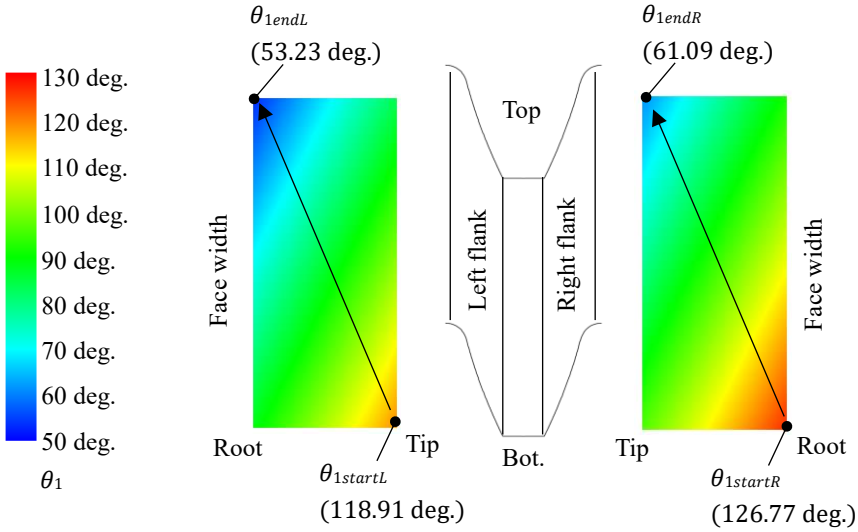

Fig. 7 Position of line of contact of right and left tooth flanks of target gear. The horizontal axis shows the normal length and the vertical axis indicates the face width position. The notation θ_{1start} is rotation angle of meshing start, θ_{1end} is rotation angle of meshing end, and subscript R denotes the right tooth flank and subscript L denotes the left tooth flank. The contour color shows the rotation angle, and the direction of the arrows indicates the direction of movement of the line of contact.

Moreover, the total contact ratio during honing can be calculated by using the θ_1. In other words, the maximum value of θ_1 is the θ_{1start} that is meshing start angle with the honing wheel, and the minimum value is the θ_{1end} that is meshing end angle with the honing wheel. The total contact ratio $\varepsilon_{\gamma 1}$ can be calculated with the following equation.

$$\varepsilon_{\gamma 1} = \frac{\theta_{1start} - \theta_{1end}}{\frac{2\pi}{z_1}} \tag{39}$$

4. Proposed honing-wheel-design method

Large tooth-flank undulations that occur during honing can make it impossible to obtain the required target gear accuracy. There are times when the honing wheel must be repeatedly designed and prototyped before the required wheel quality can be satisfied. It was observed that changing the profile shift coefficient at such times had an effect on improving tooth-flank undulations.

Soukedani reported that surface pressure fluctuations occur if the meshing-stiffness balance is not suitable, with the result that the finished tooth flank is not uniform. This occurs in the shaving process in meshing between the target gear and the shaving cutter when there is a difference in the number of teeth of the right and left tooth flanks that mesh simultaneously (Soukedani, 1989). As a solution to this problem, he showed that meshing phase differences between the right and left tooth flanks can be eliminated by using the profile shift coefficient to adjust the working pressure angle.

Based on that finding, we reasoned that the finished tooth flank is not uniform and that undulations also occur in the honing process when the meshing-stiffness balance between the honing wheel and the target gear is not suitable.

However, Soukedani's analysis method is based on a meshing calculation for point-contact of crossed helical gears, which proceeds normal to the helix angle on the base circle. Accordingly, it cannot accurately analyze differences in the number of meshing teeth of the right and left tooth flanks in the honing process, which has a line of contact inconsistent with the helix angle on the base circle.

Therefore, we applied the proposed analysis method to investigate a method of designing a profile shift coefficient

[DOI: 10.1299/jamdsm.2020jamdsm0098]

for optimizing the meshing-stiffness balance by eliminating the difference in the number of meshing teeth of the right and left tooth flanks of the honing wheel and target gear that engage simultaneously in the honing process.

4.1 Difference in number of meshing teeth of right and left tooth flanks

The total contact ratio $\varepsilon_{\gamma 1}$ calculated with Eq. (39) is divided between the integer n and the decimal s. In this process, from the θ_{1start} to the θ_{1end} meshing of n teeth occurs n times and meshing of $n+1$ teeth occurs $n+1$ times. Letting $\varphi_{n+1\ teeth}$ represent the rolling angle of $n+1$ teeth and $\varphi_{n\ teeth}$ represent that of n teeth, the respective values can be calculated with the following equations.

$$\varphi_{n+1\ teeth} = s\frac{2\pi}{z_1} \tag{40}$$

$$\varphi_{n\ teeth} = \frac{2\pi}{z_1} - \varphi_{n+1\ teeth} \equiv \frac{2\pi}{z_1}(1-s) \tag{41}$$

An example is calculated here for the specifications in Table 1. Using the analysis method explained in section 3, the meshing start angle and meshing end angle of the right tooth flank are found to be $\theta_{1startR}$ = 126.77 deg. and θ_{1endR} = 61.09 deg, respectively. Accordingly, $\varepsilon_{\gamma 1R}$ is calculated with Eq. (39) to be 4.2. $\varphi_{5\ teethR}$ and $\varphi_{4\ teethR}$ are calculated with Eqs. (40) and (41) to be 3.07 deg. and 12.58 deg., respectively. The meshing phase difference between the right and left tooth flanks is calculated to be 7.86 deg. (= 126.77 – 118.91 deg.). The analysis values will be the same for the right and left tooth flanks in the case of no tooth-flank modification and in the case where the same tooth-flank modification is applied to both tooth flanks. In contrast, in cases where the tooth-flank modification differs between the right and left tooth flanks, the analysis values will not be the same for both tooth flanks. In this analysis example here, it was assumed that the tooth flanks were not modified. The periodic diagram of the number of meshing teeth shown in Fig. 8 was created by calculating the number of meshing teeth in a given period based on the aforementioned analysis values.

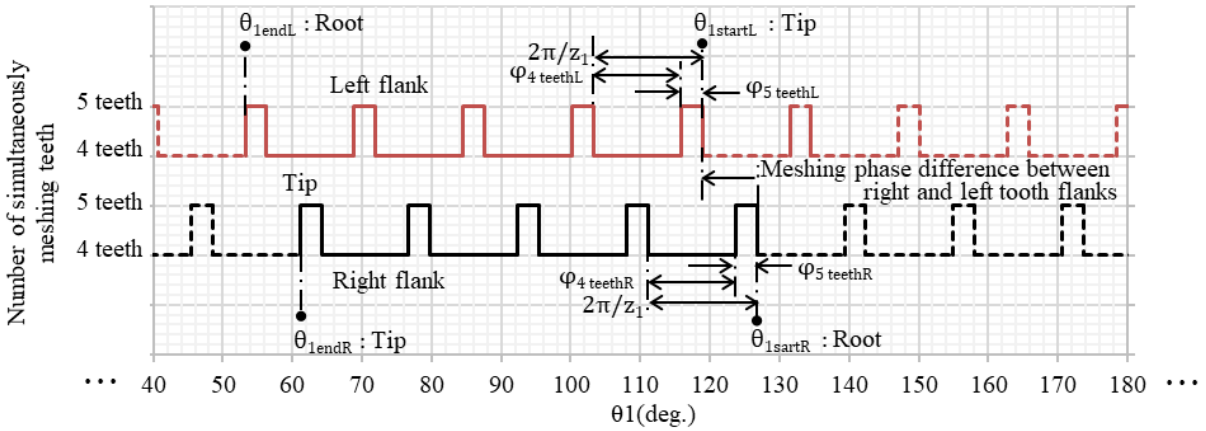

Fig. 8 Periodic diagram of the number of meshing teeth. The brown and black line show periodic diagram of the number of meshing teeth of the both left and right tooth flank, number of meshing teeth is repeated 4 teeth and 5 teeth with the meshing phase difference (7.86 deg.) between the right and left tooth flanks.

Based on Fig. 8, the number of meshing teeth of the right tooth flank at an arbitrary θ_{1R} can be calculated as shown below.

$$\varphi = (\theta_{1R} - \theta_{1startR})\frac{z_1}{2\pi} \tag{42}$$

Letting m represent the integer part of φ,
In case of ≤ 0:

$$\left|(\theta_{1R} - \theta_{1startR}) - m\frac{2\pi}{z_1}\right| \leq \varphi_{n+1\ teeth} \qquad \cdots \text{ n+1 teeth mesh} \tag{43}$$

[DOI: 10.1299/jamdsm.2020jamdsm0098]

$$\varphi_{n+1\ teeth} < \left|(\theta_{1R} - \theta_{1startR}) - m\frac{2\pi}{z_1}\right| \leq \frac{2\pi}{z_1} \quad \cdots \text{ n teeth mesh} \tag{44}$$

In case of > 0:

$$\left|(\theta_{1R} - \theta_{1startR}) - m\frac{2\pi}{z_1}\right| \leq \varphi_{n\ teeth} \quad \cdots \text{ n teeth mesh} \tag{45}$$

$$\varphi_{n\ teeth} < \left|(\theta_{1R} - \theta_{1startR}) - m\frac{2\pi}{z_1}\right| \leq \frac{2\pi}{z_1} \quad \cdots \text{ n+1 teeth mesh} \tag{46}$$

Similarly, the number of meshing teeth of the left tooth flank can be calculated for an arbitrary θ_{1L} by changing θ_{1R} to θ_{1L} in Eqs. (42) to (46) and converting $\theta_{1startR}$ to the $\theta_{1startL}$ of the left tooth flank.

Next, a method is explained for calculating the difference in the number of meshing teeth of the right and left tooth flanks during honing. Equations (42) to (46) are revised as shown below in order to calculate the number of meshing teeth of the left tooth flank at an arbitrary θ_{1R} in the interval from the start to the end of meshing of the right tooth flank.

$$\varphi = (\theta_{1R} - \theta_{1startL})\frac{z_1}{2\pi} \tag{47}$$

In case of ≤ 0:

$$\left|(\theta_{1R} - \theta_{1startL}) - m\frac{2\pi}{z_1}\right| \leq \varphi_{n+1\ teeth} \quad \cdots \text{ n+1 teeth mesh} \tag{48}$$

$$\varphi_{n+1\ teeth} < \left|(\theta_{1R} - \theta_{1startL}) - m\frac{2\pi}{z_1}\right| \leq \frac{2\pi}{z_1} \quad \cdots \text{ n teeth mesh} \tag{49}$$

In case of > 0:

$$\left|(\theta_{1R} - \theta_{1startL}) - m\frac{2\pi}{z_1}\right| \leq \varphi_{n\ teeth} \quad \cdots \text{ n teeth mesh} \tag{50}$$

$$\varphi_{n\ teeth} < \left|(\theta_{1R} - \theta_{1startL}) - m\frac{2\pi}{z_1}\right| \leq \frac{2\pi}{z_1} \quad \cdots \text{ n+1 teeth mesh} \tag{51}$$

Using the specifications in Table 1, the change in the number of meshing teeth of the right and left tooth flanks in the interval from the start to the end of meshing was calculated with Eqs. (42) to (46) for the right tooth flank and with Eqs. (47) to (51) for the left tooth flank, and the results are shown in Fig. 9.

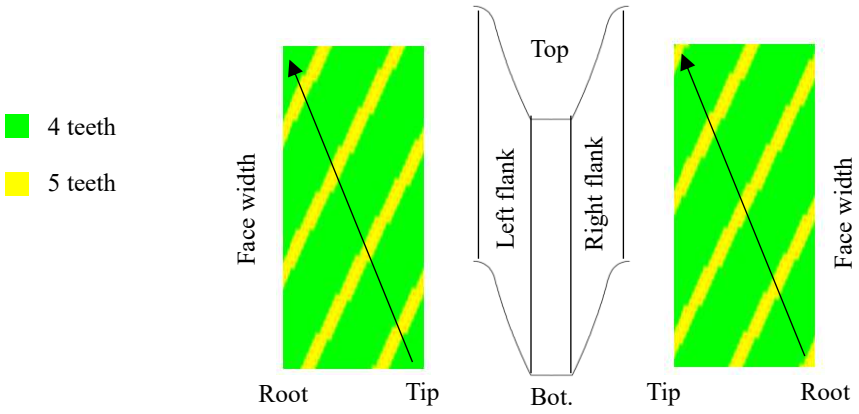

Fig. 9 Change in the number of meshing teeth of right and left tooth flanks in the interval from the start to the end of meshing. The horizontal axis shows the normal length and the vertical axis indicates the face width position. The yellow-green shows the section of 4 teeth meshing, and the yellow indicates the section of 5 teeth meshing.

The difference in the number of meshing teeth of the right tooth flank during honing can be calculated by synthesizing the change in the number of meshing teeth of the right and left tooth flanks in Fig. 9. The results are shown in Fig. 10.

[DOI: 10.1299/jamdsm.2020jamdsm0098]

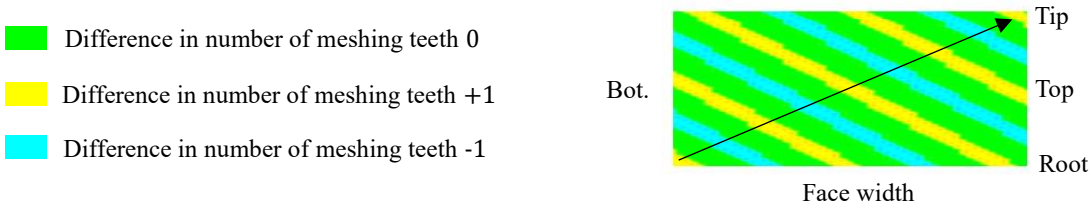

Fig. 10 Difference in the number of meshing teeth of right and left tooth flanks. The horizontal axis shows the face width position and the vertical axis indicates the normal length. The yellow-green shows difference in number of meshing teeth 0, and the yellow indicates difference in number of meshing teeth +1, and light-blue means difference in number of meshing teeth -1. The direction of the arrows indicates the direction of movement of the line of contact.

An analysis of the results in Fig. 10 reveals the possibility that a convex undulation might occur at the position of a difference in the number of meshing teeth of +1 and that a concave undulation might occur at the position of a difference of -1. The difference in the number of meshing teeth of the right and left tooth flanks in the interval from the start to the end of meshing of the left tooth flank can be calculated by changing θ_{1R} to θ_{1L} in Eqs. (42) to (46) and synthesizing the change in the number of meshing teeth of the right and left tooth flanks.

4.2 Profile shift coefficient for zero meshing phase difference between right and left tooth flanks

The design method proposed above was used to calculate a profile shift coefficient for obtaining zero meshing phase difference between the right and left tooth flanks. The method explained in subsection 4.1 was used to perform a convergence calculation to find the profile shift coefficient at which the minimum difference in the number of meshing teeth was obtained. That value was defined as the profile shift coefficient for zero meshing phase difference between the right and left tooth flanks.

Figure 11 shows the difference in the number of meshing teeth of the right and left tooth flanks obtained by using the profile shift coefficient (x_n = 0.53) for zero meshing phase difference calculated with the proposed design method based on the specifications in Table 1.

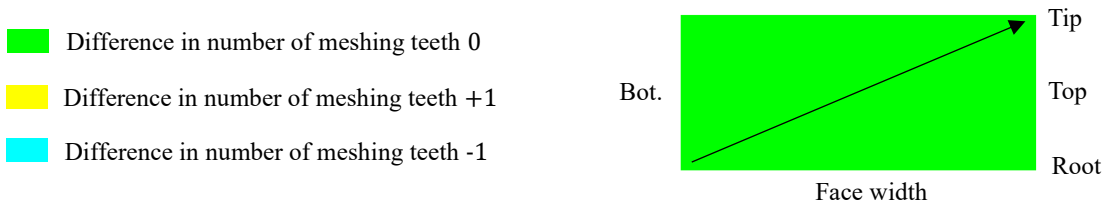

Fig. 11 Condition of zero meshing phase difference between right and left tooth flanks.

The results in Fig. 11 indicate that there was no change in the number of meshing teeth from the start to the end of meshing. It is noted that initial dressing is performed in the honing process for the purpose of truing a new honing wheel after changing wheels. It is important to design the honing-wheel geometries so that after the completion of the initial dressing a new wheel will have the desired profile shift coefficient for zero meshing phase difference between the right and left tooth flanks.

In the shaving process it is impossible to maintain a condition of zero meshing phase difference between the right and left tooth flanks from the time a new shaving cutter is installed until it is discarded. That is because the working pressure angle changes every time the cutting edges of the shaving cutter are resharpened, even if the process has been designed for zero meshing phase difference between the right and left tooth flanks. In contrast, the general practice in the honing process is to adjust the shaft angle so that the working pressure angle does not change every time the honing wheel is dressed. Consequently, a condition of zero meshing phase difference between the right and left tooth flanks can be maintained from the installation of a new honing wheel until it is discarded. Therefore, it is assumed that the idea of

[DOI: 10.1299/jamdsm.2020jamdsm0098]

designing a honing wheel with a profile shift coefficient for zero meshing phase difference between the right and left tooth flanks is an effective approach.

4.3 Influence of tooth-flank modification

Tooth-flank modification is applied to automotive transmission gears to satisfy requirements for strength and NVH performance. There are times when the modification applied to the right and left tooth flanks differs because of differences in their respective performance requirements. Owing to these circumstances, it is necessary to make clear beforehand the influence that tooth-flank modification has on the θ_1, when designing the profile shift coefficient for zero meshing phase difference between the right and left tooth flanks.

Therefore, in order to confirm the influence of tooth-flank modification, the proposed design method was used to run an analysis for various amounts of tooth-flank modification using the specifications in Table 1. The analysis conditions (amounts of tooth-flank modification) and analysis results are shown in Table 2.

Table 2 Analysis conditions (tooth-flank modification amounts) and analysis results

No.	Analysis Purpose	$f_{H\alpha}$ (μm)	$f_{f\alpha}$ (μm)	$f_{H\beta}$ (μm)	C_β (μm)	$\theta_{1startR}$ (deg.)	θ_{1endR} (deg.)	$\theta_{1startR}$ - θ_{1endR} (deg.)	Diff. (deg.)	Diff. (%)
0	Base	0	0	0	0	126.77	61.09	65.68	-	-
1	Effect of $f_{H\alpha}$	10	↑	↑	↑	126.97	61.05	65.92	0.24	1.51
2		20	↑	↑	↑	127.17	61.01	66.16	0.48	3.06
3		30	↑	↑	↑	127.36	60.98	66.38	0.70	4.47
4	Effect of $f_{f\alpha}$	0	4	0	0	127.29	61.19	66.10	0.42	2.70
5		↑	8	↑	↑	127.82	61.30	66.52	0.84	5.36
6		↑	12	↑	↑	128.35	61.40	66.95	1.27	8.14
7	Effect of $f_{H\beta}$	0	0	10	0	126.78	61.07	65.72	0.04	0.24
8		↑	↑	20	↑	126.77	61.05	65.73	0.05	0.30
9		↑	↑	30	↑	126.79	61.02	65.77	0.09	0.59
10	Effect of C_β	0	0	0	4	126.79	61.02	65.77	0.09	0.59
11		↑	↑	↑	8	126.81	61.02	65.79	0.11	0.68
12		↑	↑	↑	12	126.81	60.98	65.82	0.14	0.92

In this analysis, in addition to the $\theta_{1startR}$ and the θ_{1endR}, the $\theta_{1startR}$ - θ_{1endR} and without any tooth-flank modification were defined as reference values. The latter results are shown in Fig. 12. If the ratio was 50%, it means that the phase differed by half a pitch.

Fig. 12 Effect of tooth-flank modification on θ_1. The difference (Diff., deg.) from these values was calculated for various amounts of tooth-flank modification (table 2) and also the ratio of the difference (Diff., %) was calculated relative to one pitch (= $2\pi/z_1$).

The results clearly indicate that modification along the tooth profile had a large effect on the θ_1, whereas modification along the tooth helix had a small effect. There were cases of modification where the tooth tip relief was adopted in range of 30 to 40 μm and that effect in particular cannot be ignored. It was also observed that in cases where the tooth-flank modification differed between the right and left tooth flanks, the effect might be doubled.

[DOI: 10.1299/jamdsm.2020jamdsm0098]

The results made it clear that the profile shift coefficient for zero meshing phase difference between the right and left tooth flanks should be designed by taking into account tooth-flank modification applied to automotive transmission gears along the tooth profile.

4.4 Validation based on honing experiments

Honing experiments were conducted to verify the validity of the proposed honing-wheel-design method. The target gear used in the experiments was the secondary reduction gear of a CVT with an auxiliary transmission for use on mini-vehicles and small vehicles (Nomura et al., 2011). A cross-sectional view of the CVT is shown in Fig. 13 along with the target gear. Table 3 shows the specifications of the target gear and two honing wheels. In this experiments, dressing gear had same specifications of target gear. Table 4 shows the honing machining conditions. The honing wheel was adapted commonly used vitrified bond type, in recent years for gear honing. About target gear before honing, not only adjusted OBD after heat treatment that the target amount of tooth flank stock removal of normal direction was 0.04 mm but also adjusted tooth-flank deviation after heat treatment for target tooth-flank modification after honing.

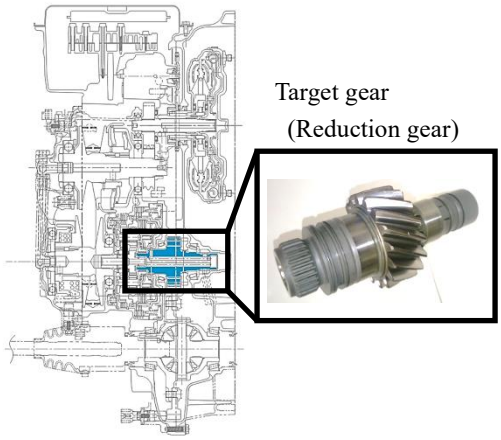

Fig. 13 CVT cross-sectional view and target gear.

Table 3 Specifications of target gear and honing wheels

			Target gear	Honing wheel A	Honing wheel B
Module	m_n	mm	2.71	←	←
Pressure angle	α_n	deg.	17.2	←	←
Helix angle	β	deg.	28.0 (RH)	38.11 (RH)	37.77 (RH)
Number of teeth	z	-	17	83	←
Tip diameter	d_a	mm	60.7	278.879	286.229
Root diameter	d_f	mm	47.049	289.611	297.771
Profile shift coeff.	x_n	-	0.3	0.340	-1.45
Face width	B	mm	23	35	←
Shaft angle	Σ	deg.	-10.00		

Table 4 Honing machining conditions

Wheel rotational speed	rpm	500
Wheel rotaional direction	-	Only CW
Amount of traverse stroke	mm	± 3
Traverse feed rate	mm/min	300
Total feed amout	mm	0.15
Feed amount / 1 stroke	mm	0.005
Amount of tooth flank stock removal of normal direction	mm	0.04

Honing wheel A was designed with a profile shift coefficient for zero meshing phase difference between the right and left tooth flanks. Honing wheel B was designed with a profile shift coefficient for a half-pitch meshing phase difference between the right and left tooth flanks. The tooth-flank modification applied to the target gear was aimed at achieving $f_{H\alpha} = 0$ µm, $f_{f\alpha} = 3$ µm, $f_{H\beta} = 0$ µm, and $C_\beta = 3$ µm for both the right and left tooth flanks (Fig. 14). The honing experiments were conducted using an asynchronous honing machine.

[DOI: 10.1299/jamdsm.2020jamdsm0098]

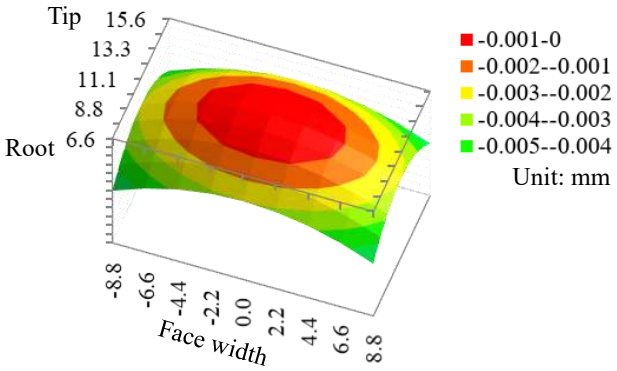

Fig. 14 Tooth-flank modification applied to the target gear for both the right and left tooth flanks.

Figure 15 shows the difference in the number of meshing teeth of the right and left tooth flanks during honing with honing wheels A and B. It is seen in the figure that there was no difference in the number of meshing teeth and zero meshing phase difference between the right and left tooth flanks when honing with honing wheel A. For honing with honing wheel B, it is seen that differences in the number of meshing teeth occurred at half pitches. In addition, because of the left and right tooth flanks have the same tooth-flank modification in this study, the difference in the number of meshing teeth of the right and left tooth flanks were the same of the right and left tooth flanks. Notes that top and bottom end are reversed for the left tooth flank.

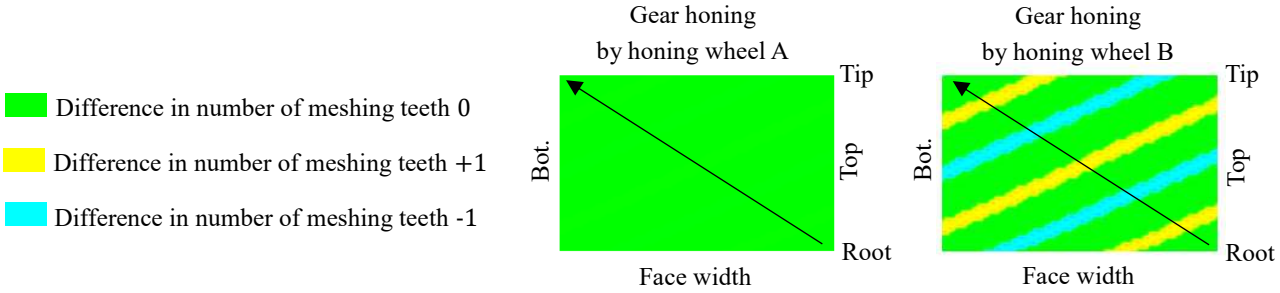

Fig. 15 Difference in number of meshing teeth of right and left tooth flanks during honing with honing wheel A and B.

Based on Fig. 15, Fig. 16 shows estimated tooth profile and tooth helix micro geometries after honing and superimposed with the results in Fig. 15. With honing wheel A can expect without tooth-flank undulations and obtaining aimed tooth flank modification. With honing wheel B is estimated that convex undulations and concave undulations occurred in both the tooth-profile and tooth-helix micro geometry at a position of +1 (red circle) and at a position of -1 (blue circle) in the difference in the number of meshing teeth, respectively.

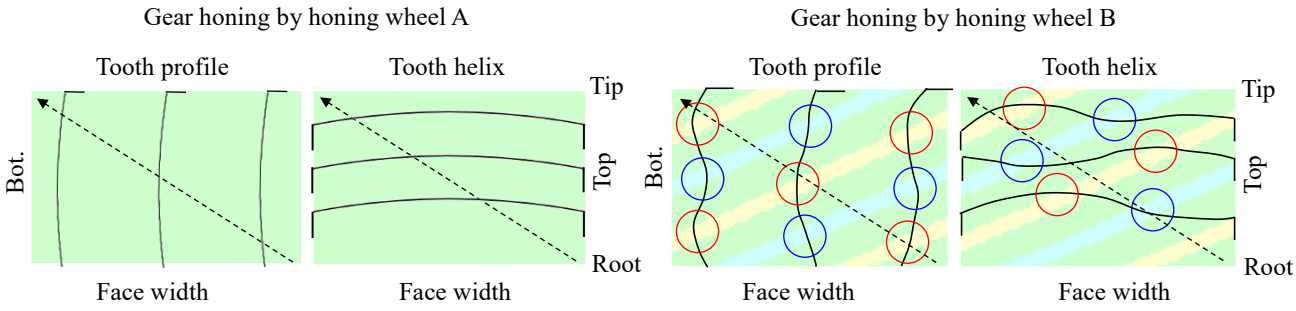

Fig. 16 Estimated tooth profile and tooth helix micro geometries after honing. Shown on the left side of the figure is the estimated tooth-profile and tooth-helix micro geometries with honing wheel A, indicated on the right side of the figure is estimated the tooth-profile and tooth-helix micro geometries with honing wheel B.

[DOI: 10.1299/jamdsm.2020jamdsm0098]

Figure 17 presents the honing experiment results obtained with honing wheel A. These results are the first measurement data after dressing and because the difference in the number of meshing teeth of the right and left tooth flanks are the same for all teeth, the one tooth is shown.

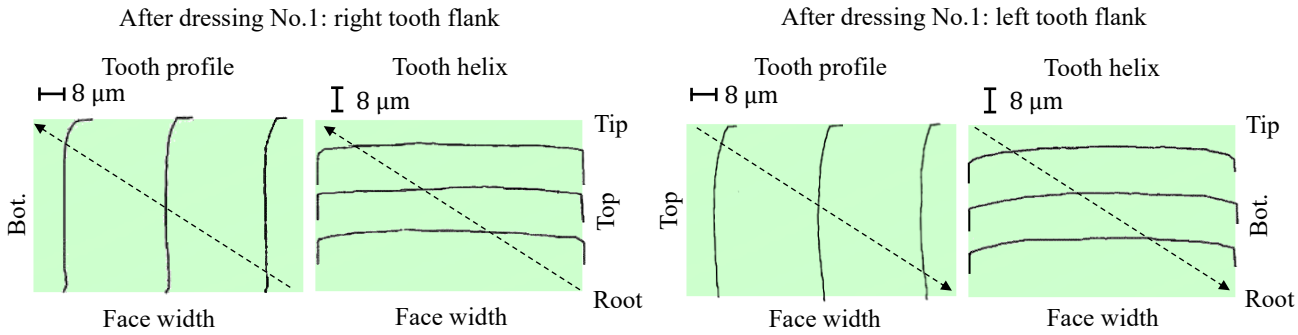

Fig. 17 Honing experiment results obtained with honing wheel A. The left side figure shows the measured tooth-profile and tooth-helix micro geometries of the right tooth flank, and the right side figure indicates the measured tooth-profile and tooth-helix micro geometries of the left tooth flank. These micro geometries aligned with the measurement position of gear accuracy and superimposed with the results in Fig. 15.

For honing wheel A that eliminated the difference in the number of meshing teeth and achieved zero meshing difference between the right and left tooth flanks, the results indicate that no undulations occurred in either the tooth-profile micro geometry or the tooth-helix micro geometry. As the results of amount of tooth-flank modification after honing, it was confirmed that at middle position of right tooth flank showed $f_{H\alpha}$ = -1 μm, $f_{f\alpha}$ = 2 μm, $f_{H\beta}$ = -1 μm, C_{β} = 2 μm and at middle position of left tooth flank showed $f_{H\alpha}$ = -2 μm, $f_{f\alpha}$ = 3 μm, $f_{H\beta}$ = 2 μm, C_{β} = 3 μm, and almost the aimed tooth-flank modification was obtained. With after dressing, N = 40 target gears were honed continuously, but no undulation occurred and good results were obtained. This confirmed that the expected results were obtained.

Next, the honing experiment results obtained with honing wheel B are shown in Fig. 18. These results are the first measurement data after dressing. With after dressing, N = 5 target gears were honed continuously and the results occurred undulation as same as the No.1 gear. Therefore the continuous honing was finished at N = 5.

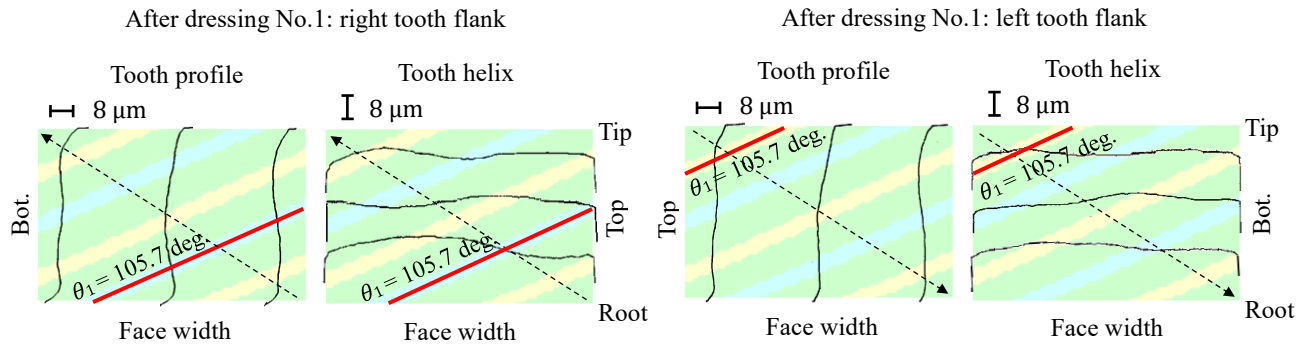

Fig. 18 Honing experiment results obtained with honing wheel B. The figure is configured similar to Fig. 17. The red line show the position of the contact line of the left and right tooth flanks at a certain rotation angle θ_1 = 105.7 deg. At this position, the right tooth flank has -1 and the left tooth flank has +1 in the difference in the number of meshing teeth.

The results indicate that convex undulations and concave undulations occurred in both the tooth-profile micro geometry and tooth-helix micro geometry at a position of +1 and at a position of -1 in the difference in the number of meshing teeth, respectively.

These honing experiment results confirmed that designing the honing wheel with a profile shift coefficient for optimizing the meshing-stiffness balance, i.e., for obtaining zero meshing phase difference between the right and left

[DOI: 10.1299/jamdsm.2020jamdsm0098]

tooth flanks, effectively suppressed tooth-flank undulations, thereby validating the proposed design method. In addition, the results also verified the validity of the analysis method explained in section 3.

Therefore, now we have adapted this proposal method in honing process for finishing CVT gears in mass production and we have obtained that tooth-flank undulations have been improved as expected. However, it has been observed that depending on the applied gear geometries, the micro geometries of the target gear show early changes (the value of $f_{f\alpha}$ increased) after dressing. This result causes shorter dressing interval, then shorter service life of a honing wheel.

Consequently, it is necessary to identify the cause of the early changes in micro geometries and develop an improved method for determining geometries of honing wheels to realize superior honing process in mass production.

5. Conclusions

The present study showed how the meshing-stiffness balance affects micro geometries of finished gear-tooth flanks in honing. The key to determining geometries of honing wheels is to maintain a balance in the meshing stiffness. Honing-wheels balancing the meshing stiffness enable the accuracy of finished gears to be stable. The present paper introduced a geometrical approach in which the mesh stiffness is balanced, and the approach constitutes a new method for determining geometries of honing wheels. The results of this study are summarized below:

(1) A calculation method was proposed, and it is a useful tool for determining geometries of a gear pair under keeping the meshing-stiffness balance.
(2) Honing experiments were conducted to assess the validity of the proposed calculation method. In the experiments, some pairs of a honing wheel and a finished gear maintain the meshing-stiffness balance, and the others do not. Both pairs induced the finished tooth forms as calculated. These results show the validity of the calculation method.
(3) A honing wheel that has a proper tooth-profile modification showed positive effects on the meshing-stiffness balance. Such a modification would also be a useful tool for determining geometries of honing wheels.

Using the proposed method, we have designed honing wheels for finishing CVT reduction gears in mass production. As a result, tooth-flank undulations have been improved as expected. This shows the validity of the proposed method. However, some honing wheels changed their tooth forms faster than expected. The change rate could depend on finished-gear geometries. This means the service life of a honing wheel becomes short and could pose a serious problem in mass production. Therefore, we should determine factors in the higher rate to develop an improved method for determining geometries of honing wheels.

References

Bergs, T., Cutting force model for gear honing, CIRP Annals Manufacturing Technology, Vol.67, Issue 1, (2018), pp.53-56.

Gunbara, H., A Study on Gear Honing Using Grinding Wheel Shaped in Internal Gear, Transactions of the JSME Lecture papers of the tokai chapter general meeting (in Japanese), Vol.49, Session ID 612, (2000), pp.353-354.

Gunbara, H., and Takenoshita, A., A Study on Gear Honing (Effect on the Tool Life the Gear Ratio between Work and Grinding Wheel), Transactions of the JSME annual meeting (in Japanese), Vol.2001.1, Session ID F-0322, (2001), pp.145-146.

Gunbara, H., A Study on Gear Honing Using Grinding Wheel Shaped in Internal Gear, Transactions of the JSME (in Japanese), Vol.69, No.679, C (2003), pp.165-170.

Gunbara, H., and Takenoshita, A., A Study on Gear Honing (Grinding Wheel Design), Transactions of the JSME annual meeting (in Japanese), Vol.2003.4, (2003), pp.39-40.

Gunbara, H., Gear Honing using Dressing Gear with Different Work – Gear' s Number of Teeth, Transactions of the JSME annual meeting (in Japanese), Vol.2004.4, Session ID 3103, (2004), pp.125-126.

Gunbara, H., Gear Honing using Dressing Gear with Different Work – Gear' s Number of Teeth, Transactions of the JSME annual meeting (in Japanese), Vol.2005.4, Session ID 2738, (2005), pp.199-200.

JSME Data Book, Gear Load Capacity, The Japan Society of Mechanical Engineers (in Japanese), (1979), pp.20-23.

Klocke, F., Gorgels, C., and Vasiliou, V., Analysis of the influence of gear dimensions on cutting speed and contact conditions during the gear honing process, Springer Link Production Engineering, Vol.3, (2009), pp.255-259.

[DOI: 10.1299/jamdsm.2020jamdsm0098]

Klocke, F., Brumm, M., and Kampka, M., Process Model for Honing Larger Gears, International Gear Conference 2014: 26th-28th August 2014, Lyon, (2014).

Kubo, A., and Umezawa, K., On the Power Transmitting Characteristics of Helical Gears with Manufacturing and Alignment Errors (1st Report): Fundamental Consideration, Transactions of the JSME (in Japanese), Vol.43, No.73, (1977) pp.2271-2783.

Meta, T., and Rathi, G., A Review On Internal Gear Honing, International Journal of Engineering Research & Technology (IJERT), Vol.2 Issue 5, (2013), pp.973-983.

Moriwaki, I., Oohashi, N., and Nakada, S., Calculations of Finished Tooth Form in Fassler Gear Honing (Removal Mechanism in Dressing and Honing), Transactions of the JSME MPT (in Japanese), Vol.2004, Session ID 422, (2004), pp.125-126.

Nakata, T., Involute Profile Shifted Gears, The Japan Society of Mechanical Engineers (in Japanese), (1949), pp.185-193.

Nonomura, R., Usuki, K., and Michioka, H., New CVT with an Auxiliary Gearbox Designed for Eco-friendliness and High Performance, JATCO Technical Review, No.10, (2011), pp.79-87.

Pascalau, N., Vuscan, I., Jiang, B., and Panc, N., RESEARCH ON INFLUENCE OF GEAR HONING PROCESS ON INVOLUTE HELICAL GEARS QUALITY, Academic Journal of Manufacturing Engineering, Vol.16, Issue 2, (2018), pp.114-119.

Rares, L., and Dana, B., Aspects of the Internal Gear Honing Process, Acta Universitatis Cibiniensis. Technical Series, Vol.70, Issue 1, (2018).

Schnider, T., THE MOST RECENT DEVELOPMENT TRENDS IN GEAR HONING, The Proceedings of the JSME international conference on motion and power transmissions, Session ID GM-13, (2009), pp.163-167.

Soukedani, K., Up Dated Technologies on Plunge Cut Shaving, NACHI-FUJIKOSHI Technical Review, Vol.45, No.1, (1989), pp.5-24.

Ueno, K., Tokawa, T., and Nishimura, Y., THE DEVELOPMENT OF GEAR HONING MACHINE, The Proceedings of the JSME international conference on motion and power transmissions, Session ID GM-6, (2001), pp.338-343.

Yokoyama, Y., and Suzuki, Y., Compliance Analysis of Gear-set, Journal of the Japan Society of Precision Engineering (in Japanese), Vol.64, No.11, (1998), pp.1585-1588.

[DOI: 10.1299/jamdsm.2020jamdsm0098]